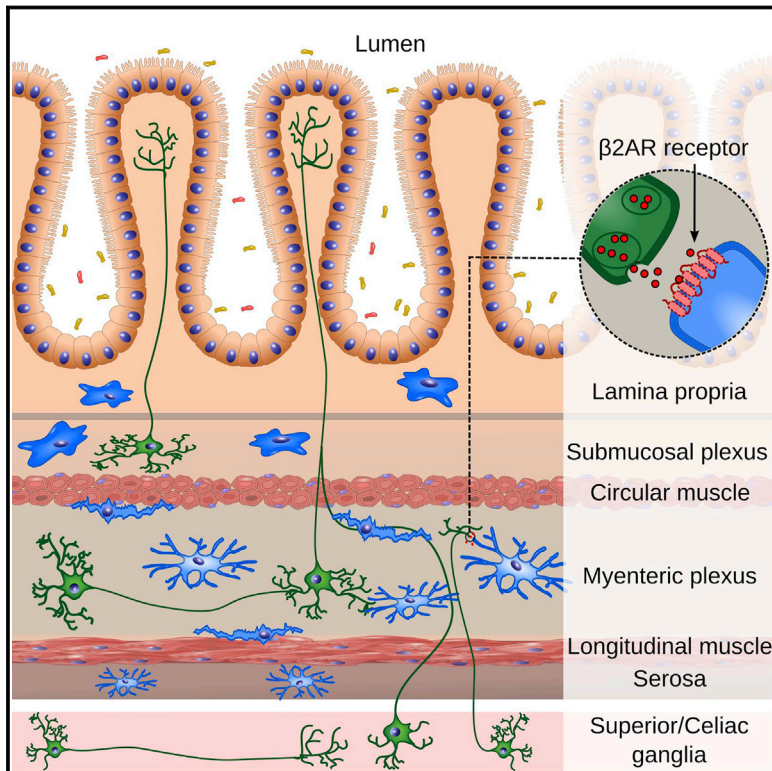


# Neuro-immune Interactions Drive Tissue Programming in Intestinal Macrophages

## Graphical Abstract



## Highlights

- Gut lamina propria and muscularis macrophages show unique intra-tissue adaptation
- Muscularis macrophages express a tissue-protective gene profile
- Gut extrinsic sympathetic innervation is activated upon distal bacterial infection
- $\beta_2$  adrenergic receptor signaling mediates MM polarization upon bacterial infection

## Authors

Ilana Gabanyi, Paul A. Muller, Linda Feighery, Thiago Y. Oliveira, Frederico A. Costa-Pinto, Daniel Mucida

## Correspondence

mucida@rockefeller.edu

## In Brief

Tissue macrophages occupying different regions of the gut exhibit a high degree of specialization and are influenced by a high density of neuronal processes in the muscularis layer, where norepinephrine released from extrinsic sympathetic innervation induces rapid tissue-protective responses to distal perturbations.

## Accession Numbers

GSE74131



# Neuro-immune Interactions Drive Tissue Programming in Intestinal Macrophages

Ilana Gabanyi,<sup>1,3,4</sup> Paul A. Muller,<sup>1,4</sup> Linda Feighery,<sup>1</sup> Thiago Y. Oliveira,<sup>2</sup> Frederico A. Costa-Pinto,<sup>1,3</sup> and Daniel Mucida<sup>1,\*</sup>

<sup>1</sup>Laboratory of Mucosal Immunology

<sup>2</sup>Laboratory of Molecular Immunology

The Rockefeller University, 1230 York Avenue, New York, NY 10065, USA

<sup>3</sup>Department of Pathology, School of Veterinary Medicine, Avenue Prof. Orlando Marques de Paiva 87, Cidade Universitária, University of São Paulo, 05508 270 São Paulo, Brazil

<sup>4</sup>Co-first author

\*Correspondence: [mucida@rockefeller.edu](mailto:mucida@rockefeller.edu)

<http://dx.doi.org/10.1016/j.cell.2015.12.023>

## SUMMARY

Proper adaptation to environmental perturbations is essential for tissue homeostasis. In the intestine, diverse environmental cues can be sensed by immune cells, which must balance resistance to microorganisms with tolerance, avoiding excess tissue damage. By applying imaging and transcriptional profiling tools, we interrogated how distinct microenvironments in the gut regulate resident macrophages. We discovered that macrophages exhibit a high degree of gene-expression specialization dependent on their proximity to the gut lumen. Lamina propria macrophages (LpMs) preferentially expressed a pro-inflammatory phenotype when compared to muscularis macrophages (MMs), which displayed a tissue-protective phenotype. Upon luminal bacterial infection, MMs further enhanced tissue-protective programs, and this was attributed to swift activation of extrinsic sympathetic neurons innervating the gut muscularis and norepinephrine signaling to  $\beta 2$  adrenergic receptors on MMs. Our results reveal unique intra-tissue macrophage specialization and identify neuro-immune communication between enteric neurons and macrophages that induces rapid tissue-protective responses to distal perturbations.

## INTRODUCTION

Intestinal tissue is continuously exposed to numerous microbe- and food-derived antigens. In order to deal with either harmless or potentially pathogenic stimulation, efficient protective responses (resistance) need to be coupled with tissue tolerance, i.e., the ability to limit disease severity induced by a given pathogen burden or inflammatory response (Råberg et al., 2007). Accordingly, while failure in innate or adaptive immunity leads to recurrent infections, deficient tolerance, or tissue repair, mechanisms result in immunopathology (Medzhitov et al., 2012; Soares et al., 2014). At the mucosal surfaces, microbial

sensing mechanisms regulate tissue repair at steady state, but in the context of infection, resistance mechanisms may lead to excessive inflammation and permanent tissue damage. Although the role of environmental cues in the adaptation of immune cells to these conditions has been increasingly appreciated, the nature of these signals and the mechanisms by which they influence immune cells are still unclear (Ayres et al., 2012; Rakoff-Nahoum et al., 2004).

Tissue-resident macrophages represent a highly heterogeneous cell population able to sense and quickly adapt to environmental cues (Hashimoto et al., 2013; Lavin et al., 2014; Nguyen et al., 2011; Okabe and Medzhitov, 2014; Wang et al., 2012, 2015). A vast network of macrophages populates intestinal tissue, playing either protective or tolerogenic roles, depending on the context (Bogunovic et al., 2009; Denning et al., 2007; Parkhurst et al., 2013; Zigmond et al., 2014). Mucosal, or lamina propria macrophages (LpMs), are located underneath the epithelial layer and are in close proximity to the gut lumen (Farache et al., 2013; Mazzini et al., 2014; Zigmond et al., 2014). Muscularis macrophages (MMs), on the other hand, are located underneath the submucosal region between circular and longitudinal muscle layers, comparatively distant from luminal stimulation (Bogunovic et al., 2009). Early studies suggested that LpMs play an important role by sampling luminal bacteria and initiating adaptive immune responses to clear pathogenic bacteria (Niess et al., 2005). Additionally, LpMs are thought to initiate a cascade of events involved in tolerance to dietary antigens (Hadis et al., 2011; Mazzini et al., 2014). In contrast, a recent study indicated that MMs regulate the activity of enteric neurons and peristalsis, although this macrophage population remains largely uncharacterized (Muller et al., 2014). It also remains to be defined how distinct programs in a specific cell lineage can arise within different compartments of the same tissue.

Using live multi-photon microscopy and tissue-clearing imaging techniques, we observed distinct cell dynamics and morphological features between LpMs and MMs. Unique intra-tissue specialization of these two macrophage populations was confirmed by transcriptional profiling tools, which showed that LpMs preferentially expressed a pro-inflammatory phenotype while MMs displayed a tissue-protective gene-expression profile at steady state. Following luminal infection, gut macrophages exhibited distinct responses according to their location, further

reinforcing their steady state tissue signature. This divergent transcriptional profile was in part dependent on norepinephrine signaling via  $\beta_2$  adrenergic receptors ( $\beta_2$ ARs), which are highly expressed on MMs. Correspondingly, using a gene reporter and transcriptional profiling we observed that luminal infection activates tyrosine hydroxylase-expressing neurons in the sympathetic ganglia innervating the intestine. This work identifies a mechanism by which interaction between intestinal neurons and macrophages can mediate intra-tissue adaptation in response to distal environmental perturbations, forming a cellular network possibly involved in maintaining the balance between resistance and tolerance.

## RESULTS

### Distinct Morphological Features and Cell Dynamics Inherent to Lamina Propria and Muscularis Macrophages

To obtain a deep-tissue, 3D view of gut-resident macrophage distribution within the intact intestinal tissue, we performed whole-mount immunolabeling, utilizing a tool referred to as immunolabeling-enabled three-dimensional imaging of solvent-cleared organs (iDISCO) (Renier et al., 2014). Small intestine sections from *Cx3cr1*<sup>GFP/+</sup> macrophage reporter mice (Niess et al., 2005) were stained with anti-GFP antibodies and visualized using light-sheet microscopy. Resulting images revealed dense macrophage networks throughout the tissue layers and particularly concentrated in the lamina propria (LpMs) and muscularis (MMs) regions, suggesting compartmentalization of gut macrophage populations (Figure 1A; Movie S1A). To gain insight into cell dynamics in these two distinct layers of the intestinal wall of live animals, we utilized intravital multi-photon microscopy (IVM) (Farache et al., 2013). We analyzed *Itgax*<sup>eYFP</sup> (CD11c<sup>eYFP</sup>) and *Cx3cr1*<sup>GFP/+</sup> reporter mice side-by-side, which allow the visualization of intestinal antigen-presenting cells (APCs) and macrophage populations, respectively (Farache et al., 2013; Niess et al., 2005). Comparison between macrophages (CD11c<sup>+</sup> and/or CX<sub>3</sub>CR1<sup>+</sup>) residing in the lamina propria and muscularis compartments revealed distinct morphologies inherent to these populations, including varied displacement and dendrite extension patterns. LpMs exhibited slow displacement, while MMs were primarily static, and MMs possessed greater dendrite ramifications than LpMs but reduced dendritic extension movements (Figures 1B and 1C; Movies S1B and S1C). Among the MM population, we observed at least two morphologically distinct sub-populations: bipolar and stellate cells (Phillips and Powley, 2012) (Figure 1D; Movies S1D and S1E). In general, bipolar cells produced small pseudopodia along the length of the cell body, ~0.2–0.8  $\mu$ m in size. Stellate cells also exhibited these pseudopodia, but they also displayed constant extensions and retractions of their dendritiform processes. These observations suggest that macrophages within distinct compartments of the gut display different morphologies and cellular dynamics.

Since, in addition to macrophages, the gut wall also contains several DC subpopulations (Bogunovic et al., 2009; Schreiber et al., 2013), we complemented this cell surface marker-based lineage classification with complementary ontogeny strategies.

We targeted the macrophage/monocyte lineage using *Lyz2*<sup>Cre</sup> x *Csf1*<sup>tsi-DTR</sup> (*Lyz2*<sup>csf1r-DTR</sup>) and the pre-DC-derived lineage using *Zbtb46*<sup>DTR</sup> (zDC<sup>DTR</sup>) mice (Schreiber et al., 2013). Administration of diphtheria toxin (DT) to *Lyz2*<sup>csf1r-DTR</sup> mice leads to broad, rapid depletion of monocytes, monocyte- and yolk sac-derived tissue macrophages and inflammatory DCs that lasts for at least 36 hr. Complementarily, DT-injected zDC<sup>DTR</sup> mice show rapid and virtually complete loss of classical DCs (cDCs) (Schreiber et al., 2013). We generated bone marrow chimeras (BMC) from *Cx3cr1*<sup>GFP/+</sup> reporter mice crossed to *Lyz2*<sup>csf1r-DTR</sup>, zDC<sup>DTR</sup> or wild-type (WT) controls to allow CX<sub>3</sub>CR1<sup>+</sup> APCs not targeted by DT to be visualized by the expression of GFP. At 12 hr post-final DT injection, we observed a drastic reduction in GFP<sup>+</sup> cells in the muscularis and lamina propria of *Lyz2*<sup>csf1r-DTR</sup> when compared to WT controls or zDC<sup>DTR</sup> mice, indicating that the great majority of CX<sub>3</sub>CR1<sup>+</sup> cells in these layers belongs to the monocyte/macrophage lineage (Figure 1E). In contrast, DT administration to CD11c<sup>eYFP</sup>-<sup>P</sup>*Lyz2*<sup>csf1r-DTR</sup> BMC resulted in a drastic reduction in YFP<sup>+</sup> cells in the muscularis, but only mild reduction in YFP<sup>+</sup> in the lamina propria (Figure S1). These data indicate that CX<sub>3</sub>CR1-based strategies faithfully label macrophages throughout the gut tissue, while CD11c also labels non-monocyte/macrophages in the lamina propria and can therefore only be used to visualize MMs.

By combining methods to visualize deep-tissue structures with intersectional genetics and live imaging, these experiments establish tissue segregation, distinct morphology, and cell dynamics of macrophages residing within distinct microenvironments in the intestinal tissue.

### Intra-tissue Specialization of Lamina Propria and Muscularis Macrophages

To address whether the morphological and cell dynamics characteristics of gut macrophages correspond to divergent tissue-specific adaptation, we analyzed the transcriptomes of LpMs and MMs. RNA sequencing (RNA-seq) analysis of sorted (live, CD45<sup>+</sup>Lineage<sup>-</sup>MHCII<sup>+</sup>CD11b<sup>+</sup>CD11c<sup>+</sup>CD103<sup>-</sup>) cells at steady state revealed significant differences between LpM and MM cells in genes related to immune and metabolic processes (Figures 2A, 2E, and S2; Table S1). MM preferentially expressed tissue-protective and wound healing genes, such as *Retnla* (encoding Fizz1), *Mrc1*, *Cd163*, and *Ii10* and increased levels of the co-stimulatory molecule CD86 when compared to macrophages isolated from the lamina propria (Figures 2A–2C and 2E), and overall resemble alternatively activated (M2) macrophages (Van Dyken and Locksley, 2013). Analysis of the ImmGen database (Gautier et al., 2012), as well as flow cytometry and qPCR further confirmed this trend, also indicating that LpMs preferentially expressed pro-inflammatory, or M1, genes with increased oxidative burst and increased CD80 expression when compared to MMs (Figures 2B and 2C).

The above data demonstrate an intra-tissue specialization among intestinal macrophages with potential for modified responses in specific microenvironments. To determine whether the basal differences between intestinal macrophages are maintained during responses to a pathogen, we sorted LpMs and MMs 2 hr post-intra-gastric exposure to mutant strains of

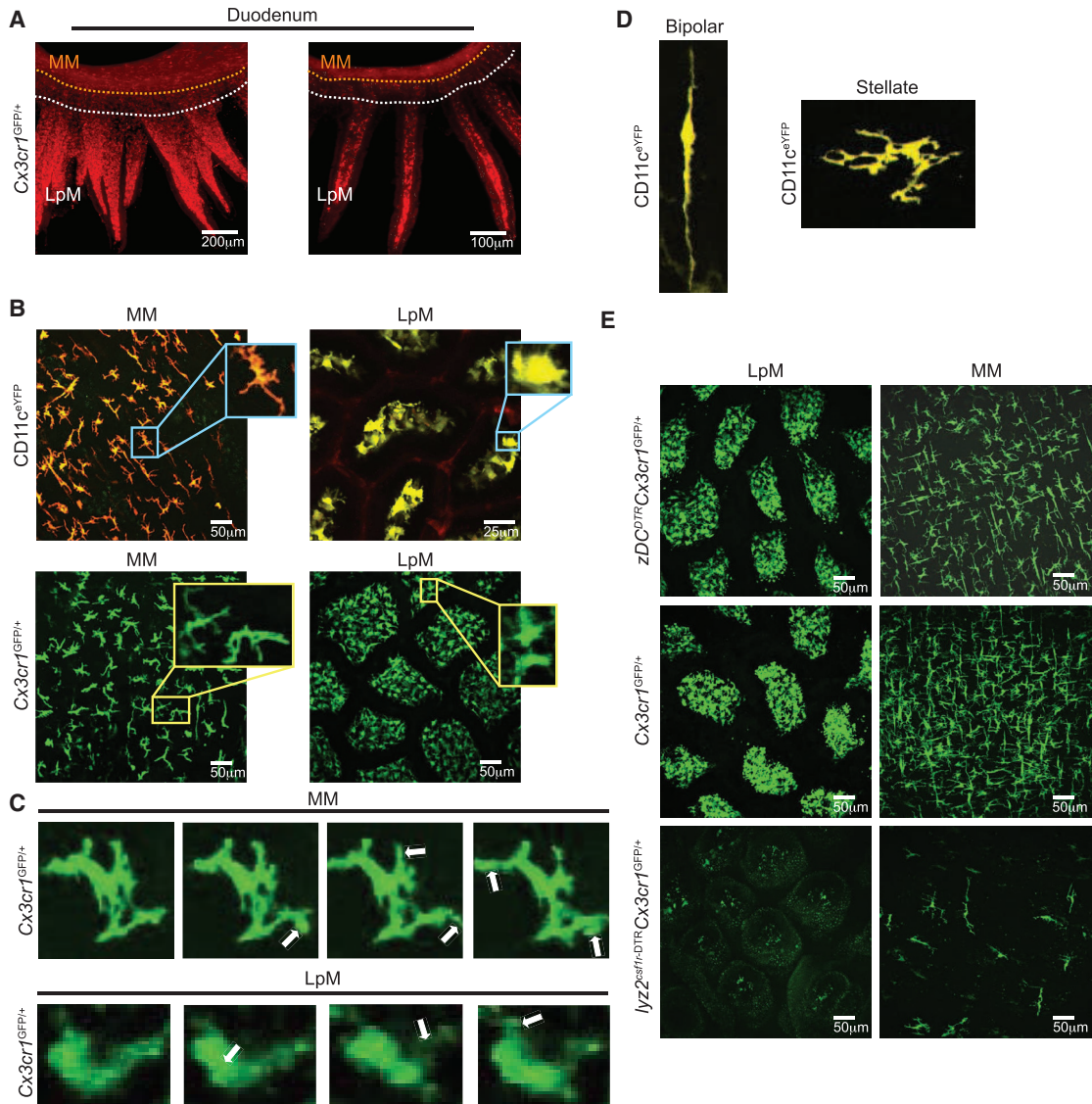


### Figure 1. MMs Differ from LpMs in Morphology and Cell Dynamics

(A) Whole-mount imaging (iDISCO) of gut macrophages in the duodenum section isolated from *Cx3cr1*<sup>GFP/+</sup> reporter mouse and stained with anti-GFP. Left: still image from a 3D reconstruction (see [Movie S1A](#)). Right: Imaris-generated orthogonal slice. Image is representative of two similar experiments with sections obtained from duodenum, jejunum, and ileum.

(B) Images from IVM of the ileum muscularis (left) and lamina propria (right) of live *CD11c*<sup>eYFP</sup> (upper panels) and *Cx3cr1*<sup>GFP/+</sup> (lower panels) mice. Insets depict different morphological features of APCs in each region (see also [Movies S1B](#) and [S1C](#)). Images are representative of at least five similar experiments.

(C) Images from IVM of the ileum muscularis (upper panels) and lamina propria (lower panels) of live *Cx3cr1*<sup>GFP/+</sup> mice. White arrows indicate morphologic changes over 15–20 min. Images are representative of at least five similar experiments.

(D) Images from IVM of the ileum muscularis isolated from *CD11c*<sup>eYFP</sup> mice depicting different morphological features of MMs: bipolar cell (left) and stellate cell (right) (see also [Movies S1D](#) and [S1E](#)). Images are representative of at least five similar experiments.

(E) Multi-photon microscopy images of freshly isolated ileum lamina propria (left column) and muscularis (right column) of *Cx3cr1*<sup>GFP/+</sup> (middle row), *zDC*<sup>DTR</sup> *Cx3cr1*<sup>GFP/+</sup> (upper row), and *Lyz2*<sup>csf1r-DTR</sup> *Cx3cr1*<sup>GFP/+</sup> (lower row) mice 12 hr post-final DT administration. Images are representative of three similar experiments. See also [Figure S1](#) and [Movie S1](#).

*Salmonella typhimurium*, *Spib*, and *invA*, which exhibit impaired proliferation or invasiveness, respectively, due to mutations in the type-III secretion system ([Tsolis et al., 1999](#)). We chose to study non-pathogenic or non-invasive bacteria strains since WT *Salmonella* Typhimurium quickly invades and damages the

intestinal epithelium, hindering our objective to compare macrophages located in different regions of intact intestinal tissue. A 2 hr time-point was chosen to represent the earliest detection point for immediate early gene (IEG) responses in macrophages ([Ghisletti et al., 2010](#)). Following gavage with the *Spib* mutant,

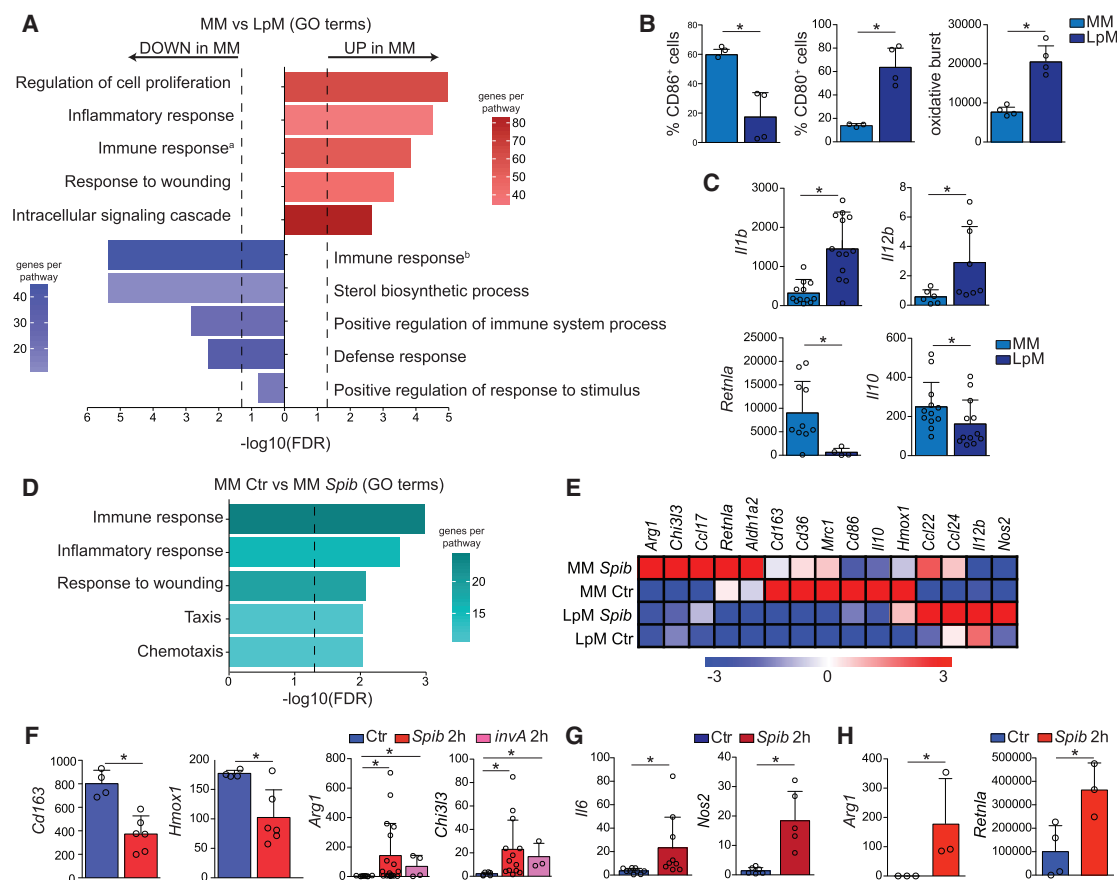


**Figure 2. MMs and LpMs Exhibit Distinct Gene Expression Signatures**

(A–G) MMs and LpMs were isolated from the small intestine muscularis *externa* and mucosal layers, respectively, of WT mice and sorted as live (Aqua<sup>-</sup>) CD45<sup>+</sup>Lin<sup>-</sup>MHCII<sup>+</sup>F4/80<sup>+</sup>CD11b<sup>+</sup>CD11c<sup>-</sup>CD103<sup>-</sup>. (A) Annotated gene ontology (GO) biological processes were assigned to genes differentially expressed by MMs when compared to LpMs, determined by RNA-seq. n = 2 per condition. (B) Flow cytometry analysis of CD80 and CD86 expression and oxidative burst by MMs and LpMs. Data are representative of at least two independent experiments, n = 4. (C) Expression of mRNA for *Il1b*, *Il12b*, *Retnla*, and *Il10* by MMs and LpMs determined by qPCR, presented relative to housekeeping gene *Rpl32* expression. n = 6–12, pooled data. (D) Annotated GO biological processes were assigned to genes differentially expressed by MMs 2 hr post-intragastric exposure to *Spib* when compared to MMs isolated from naive mice, determined by RNA-seq. n = 2 per condition. (E) Heat map of representative M1- and M2-related genes assigned to genes differentially expressed by MMs and LpMs 2 hr post-intragastric exposure to *Spib*, determined by RNA-seq. n = 2 per condition. (F and G) Expression of mRNA for various genes by (F) MMs and (G) LpMs 2 hr post-intragastric exposure to *Spib* or *invA Salmonella* Typhimurium mutant strains determined by qPCR, presented relative to *Rpl32* expression. (F and G) n = 4–13; pooled data. (H) Expression of polysome-associated mRNA from small intestine muscularis of *Lyz2*<sup>RiboTag</sup> mice 2 hr post-intragastric exposure to *Spib* determined by qPCR, presented relative to *Gapdh*. n = 3 per condition. Data were analyzed by unpaired t test and are shown as average ± SD; \*p < 0.05.

See also Figure S2 and Table S1, worksheets a–c.

we observed significant further upregulation in some M2-associated genes in MMs, particularly *Arg1* and *Chi3l3* (encoding YM1). While *Cd163* and *Hmox1* were downregulated, they were still expressed at higher or similar levels than in LpMs, respectively (Figures 2D–2F; Table S1). Of note, whereas we observed variability in the expression of some IEG's, particularly *Arg1*, among different animals, MMs from non-infected mice consistently did not express these genes (Figure 2F). In contrast, very few changes in gene expression were observed in LpMs upon intragastric exposure to *Spib*, and these changes were mostly restricted to M1-associated genes, including *Nos2* and *Il6* (Figures 2E and 2G).

To corroborate observed changes in MM gene expression profile using an independent approach, we conducted cell

type-specific ribosomal profiling. This approach eliminates the need for cell sorting to purify sub-populations, thus reducing processing time and variability. We chose to specifically focus on actively translated mRNAs by interbreeding mice expressing *Cre* under the *Lyz2* promoter with mice carrying a targeted knockin into the ribosomal protein L22 gene (RiboTag). *Cre*-mediated activation in this system creates an HA-tagged ribosomal protein, enabling affinity-tagged purification and identification of actively translated ribosome-bound mRNAs in macrophages from intact tissues (Sanz et al., 2009). Analysis of intestinal muscularis from *Lyz2*<sup>RiboTag</sup> mice confirmed high levels of active translation of M2-related genes in steady state in MMs, particularly *Retnla*. Importantly, intragastric inoculation of mice with *Spib* rapidly led to upregulation of *Arg1* as well as

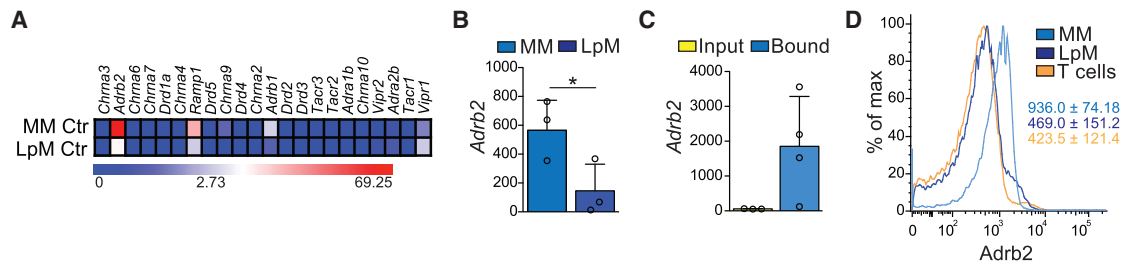


### Figure 3. MMs Preferentially Express $\beta_2$ ARs

(A) Heat map of genes for neurotransmitter receptors expressed by sorted small intestine MMs and LpMs isolated from naive WT mice under steady state conditions, determined by RNA-seq.  $n = 2$  per condition.

(B) Expression of mRNA for *Adrb2* by sorted small intestine MMs and LpMs isolated from naive WT mice, determined by qPCR, presented relative to *Rpl32* expression. Data are representative of two independent experiments,  $n = 3$ .

(C) Expression of polysome-associated mRNA from small intestine muscularis of *Lyz2<sup>RiboTag</sup>* mice, determined by qPCR, presented relative to *Gapdh* expression. Input,  $n = 3$ , bound,  $n = 4$ .

(D) Representative flow cytometry histogram for  $\beta_2$ AR expression by small intestine MMs, LpMs, and peripheral T cells isolated from naive WT mice. Histograms are representative of two independent experiments,  $n = 3$ . Data were analyzed by unpaired t test and are shown as average  $\pm$  SD; \* $p \leq 0.05$ . See also Figure S2.

*Retnla* (Figure 2H). These results suggest that unique microenvironmental cues influence the specialization of gut-resident macrophages and that this specialization is reinforced upon infection.

### $\beta_2$ AR-Positive Muscularis Macrophages Reside in Close Proximity to Firing Neurons

We next asked whether specific environmental signals, particularly soluble factors, were responsible for the distinct gene expression profiles and responses to luminal insults by LpM and MM populations. Gene expression profiling of LpM and MM cells indicated that pro- or anti-inflammatory cytokine-, TLR-, or FcR-mediated signaling did not segregate these populations, especially considering the canonical M1 (IFN- $\gamma$ R, IFN- $\alpha$ R, IL-1R, TLR4) or M2 (Fc $\gamma$ R1b, IL-4R $\alpha$ , IL-10R $\alpha$ , ST2 [encoded by *Il1rl1*]) polarizing receptors (Figure S2B) (Gautier et al., 2012). Given their distinct locations near the lumen (LpM) or near neuronal networks (MM) (Kinoshita et al., 2007; Muller et al., 2014; Phillips and Powley, 2012), we next asked whether these macrophage populations differentially expressed neurotransmitter or neuropeptide receptors. MMs expressed high levels of *Adrb2* (encoding  $\beta_2$  adrenergic receptors [AR]), and this was also among the most significantly differentially-expressed genes between MM and LpM populations in the ImmGen database (Figure 3A) (Gautier et al., 2012). We confirmed these results by performing qPCR on sorted cells isolated from WT mice and on HA-bound polysomes of intestinal muscularis tissue isolated from *Lyz2<sup>RiboTag</sup>* mice (Figures 3B and 3C). Furthermore, flow-cytometric analysis of LpMs and MMs isolated from the small intestine of WT mice revealed high levels of membrane  $\beta_2$ AR expression in MMs and lower, albeit detectable, expression of  $\beta_2$ ARs by LpMs (Figure 3D).

The near immediate gene-expression response of MMs to distal luminal stimuli, along with their selective expression of neurotransmitter receptors, suggested that their specific location in close proximity to neuronal networks could be influencing their activity. We therefore chose to characterize this neuron-rich microenvironment and how it interacts with gut macro-

phages. To that end, we developed multiple genetic labeling tools, allowing for concomitant and dynamic visualization of these cell types. To gain insight into neuron-macrophage interactions in live animals, we first generated a more specific enteric neuronal-associated reporter by interbreeding *Rosa26<sup>Isl-tdTomato</sup>* with *Hand2<sup>Cre</sup>* (*Hand2<sup>Tomato</sup>*) mice (Hender-shot et al., 2007). These mice express *Cre* recombinase under the promoter of *Hand2*, a helix-loop-helix transcription factor with an established role in development of the enteric-associated neurons (EAN) (Barron et al., 2011). *Cre*-mediated removal of the *stop* cassette generated bright red fluorescence that allowed the visualization and tracking of *Hand2*-expressing cells, mostly restricted to EAN (Figure 4A). These mice were crossed with *Cx3cr1<sup>GFP/+</sup>* reporter mice for tracking intestinal macrophages, and the resulting offspring were used for concomitant EAN-macrophage visualization. We observed that most of the CX<sub>3</sub>CR1<sup>+</sup> cells in the muscular region were in close proximity to neuronal cell bodies or processes of the myenteric ganglia (Figure 4B; Movie S2A). We distinguished four layers of muscularis macrophages: serosal/longitudinal, myenteric plexus, circular muscle, and deep muscular plexus (Figures 4C and 4D). Serosal macrophages do not appear to be associated with enteric neurons and tend to be larger in size when compared to the other layers (Figure 4D). Myenteric plexus MMs are in close proximity to neuronal cell bodies and some nerve fibers, while MMs within the circular muscle and deep muscular plexus have their cell bodies running in parallel to the nerve fibers (Figure 4D).

To complement our cell dynamics analysis, we assessed neuronal activation in areas where MMs were co-localized with EAN utilizing a mouse strain containing a genetically encoded, *Cre*-dependent calcium indicator (GCaMP3) (Zariwala et al., 2012). Analysis of *Hand2<sup>Cre</sup>*  $\times$  *Rosa26<sup>Isl-GCaMP3</sup>* (*Hand2<sup>GCaMP3</sup>*)  $\times$  *CD11c<sup>eYFP</sup>* mice revealed neuronal activity in very close proximity to MMs in the myenteric plexus (Figure 4E; Movie S2B). Taken together, these data indicate that MMs that express  $\beta_2$ AR reside in close proximity to active neurons in the intestine.

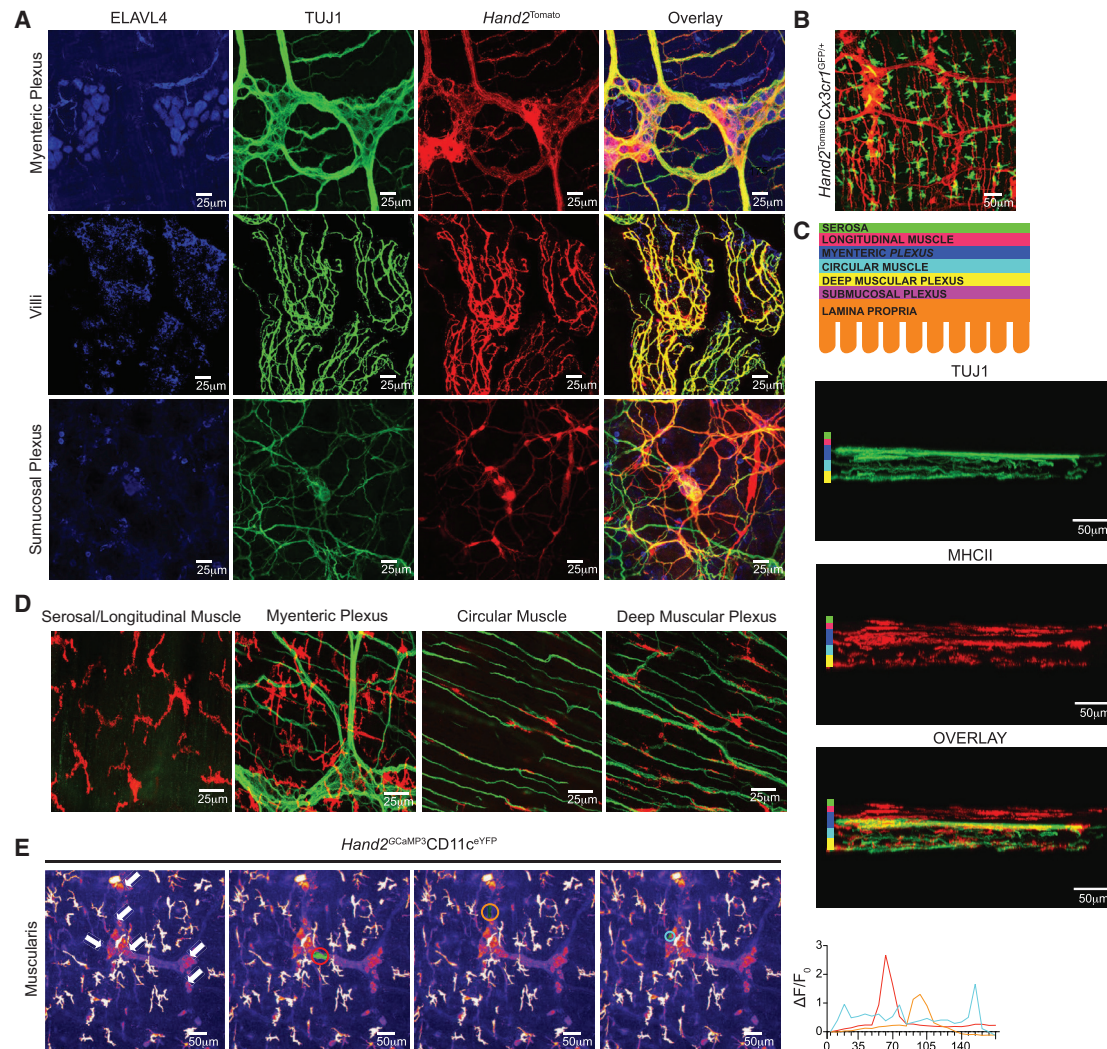


**Figure 4. MMs Are Closely Associated with Active Neurons**

(A) Confocal images from the myenteric plexus (upper panels), villi (middle panels) and submucosal plexus (lower panels) isolated from naive *Hand2<sup>Cre</sup> Rosa26<sup>lsl-tdTomato</sup>* (*Hand2<sup>Tomato</sup>*) mice and stained using anti-ELAVL4 (HuC/D) and anti-TUJ1 ( $\beta$ III tubulin) antibodies. Images are representative of 2 similar experiments with sections obtained from duodenum, jejunum, and ileum.

(B) Image from IVM of the ileum muscularis of live *Hand2<sup>Tomato</sup>Cx3cr1<sup>GFP/+</sup>* mice (see [Movie S2A](#)). Image is representative of at least ten similar experiments.

(C and D) Confocal images from the ileum isolated from naive WT mice stained using anti-TUJ1 ( $\beta$ III tubulin) and anti-MHCII antibodies. (C, upper panel) Schematic of layers of different small intestine muscularis. (C, lower panel) Four layers of muscularis orthogonal slices are depicted according to the color scheme. (D) Images depict macrophages occupying each of the four layers: serosal/longitudinal muscle, myenteric plexus, circular muscle, and deep muscular plexus. Images are representative of at least three independent experiments.

(E) Images from IVM of the ileum muscularis of live *Hand2<sup>GCaMP3</sup>CD11c<sup>eYFP</sup>* mice over 3 min. White arrows indicate neurons labeled with GCaMP3, and colored regions of interest (ROI) highlight neural activity (see also [Movie S2B](#)). Corresponding colored traces plot changes in fluorescence ( $\Delta F$ ) of ROI per time frame (in seconds), with an increase in fluorescence indicative of  $Ca^{2+}$  influx and depolarization (right). Images are representative of at least three independent experiments.

See also [Movie S2](#).

### Rapid Activation of Catecholaminergic Neurons Occurs upon Luminal Infection

We next sought to characterize the specific neurochemical pathway involved in the activation of  $\beta_2AR^+$  MMs by defining the source of norepinephrine (NE) in the gut muscularis. Although neurons are the most studied sources for catecholamines, recent studies have shown that myeloid cells, including macro-

phages, can also produce these neurotransmitters. Specifically, alternatively-activated macrophages involved in the regulation of thermogenesis were shown to express tyrosine hydroxylase (TH) and produce NE ([Nguyen et al., 2011](#)). To better characterize possible neuronal and non-neuronal sources for NE in the gut, we first interbred *Rosa26<sup>lsl-tdTomato</sup>* with *Th<sup>Cre</sup>* mice (*Th<sup>Tomato</sup>*) as a fate-mapping strategy to visualize cells that express TH at

any point during development. Immunofluorescence microscopy analysis of *Th<sup>Tomato</sup>* mice suggested that neurons, not myeloid cells, were the main source of NE within intestinal tissue, as revealed by extensive Tomato co-localization with the pan-neuronal marker ELAVL4 in the muscularis and absence of Tomato expression by myeloid cells (Figure 5A), data confirmed by flow cytometric analysis (data not shown). To visualize cells actively expressing TH, we also performed ex vivo staining for TH and additional neuronal or myeloid markers. Again, TH staining was restricted to the neuronal compartment, particularly the fibers near MMs (Figure 5B). To visualize the catecholaminergic innervation throughout the intestinal tissue and how it permeates gut macrophages, we performed iDISCO in small intestinal sections from *Cx3cr1<sup>GFP/+</sup>* reporter mice, co-stained with anti-GFP and anti-TH antibodies. Light-sheet microscopy analysis revealed intense TH<sup>+</sup> innervation in the gut muscularis, but sparse labeling in the lamina propria (Figures 5C and 5D; Movies S3A and S3B). We also observed TH<sup>+</sup> processes extending from the muscularis region (Figures 5C and 5E; Movie S3C), suggesting an extrinsic nature for this innervation.

After defining catecholaminergic innervation as the probable source of NE in the MM microenvironment, we next characterized the intrinsic (cell bodies that lie within the intestinal tissue) versus extrinsic (cell bodies that lie outside of the intestinal tissue) nature of these neuronal processes (Furness et al., 1999). In order to identify and visualize the sympathetic innervation of the intestine, we developed general fate-mapping strategies by crossing *Rosa26<sup>Isl-tdTomato</sup>* with *Snap25<sup>Cre</sup>* (pan-neuronal) mice (Harris et al., 2014) or with *Wnt1<sup>Cre</sup>* (neural crest-derived) (Danielian et al., 1998) mice, respectively, which revealed the superior mesenteric-celiac ganglia (SMG-CG) (Figure 5F and data not shown). Immunolabeling of the SMG-CG showed a dense network of ELAVL4 and TH<sup>+</sup> neurons extending processes toward the gut (Figures 5G and 5H; Movie S3D). Consistent with this, staining for dopamine  $\beta$ -hydroxylase (DBH), which converts dopamine into norepinephrine, revealed punctate labeling restricted to ganglia and nerve fibers in the myenteric and submucosal plexuses, while extrinsic sympathetic neurons displayed signal in their cytoplasm (Figure S3). This observation indicates that at least part of the TH staining observed in the muscularis was of an extrinsic nature, as previously suggested (Li et al., 2010).

To address whether intrinsic innervation also contributed to the catecholaminergic response in the muscle, we generated a broad neuronal RiboTag strain by crossing *Rpl22<sup>Isl-HA</sup>* with *Snap25<sup>Cre</sup>* (*Snap25<sup>RiboTag</sup>*) mice. Analysis of HA-bound fractions from the muscularis and the SMG-CG revealed high expression of both *Th* and *Dbh* by SMG-CG but a lack of expression in the myenteric plexus (Figure 6A). We therefore concluded that a majority of the NE release in the gut muscularis microenvironment is derived from extrinsic sympathetic innervation.

One of the consequences of NE in the muscularis region is the relaxation of intestinal smooth muscle (Pullinger et al., 2010). Consistent with this effect, we observed a significant impairment of gastrointestinal motility following oral gavage with *Salmonella* Typhimurium mutant *Spib* (Figure 6B). Additionally, quantification of NE in the cecal contents also indicated increased NE release in the intestinal tissue upon *Spib* infection (Figure S4). Finally, to confirm catecholaminergic neuronal activation after

luminal infection, we measured c-Fos activation using *Fos<sup>GFP</sup>* reporter mice. Oral administration of *Spib* resulted in pronounced activation of SMG-CG ganglia neurons and undetectable (or non-neuronal) c-Fos expression in the intestinal muscularis (Figures 6C, 6D, and S4). Collectively, these data suggest that enteric infections activate gut extrinsic sympathetic innervation resulting in NE release within the muscular region and signaling through  $\beta_2$ ARs in MMs.

### $\beta_2$ AR-Mediates Alternative Activation of Intestinal Macrophages

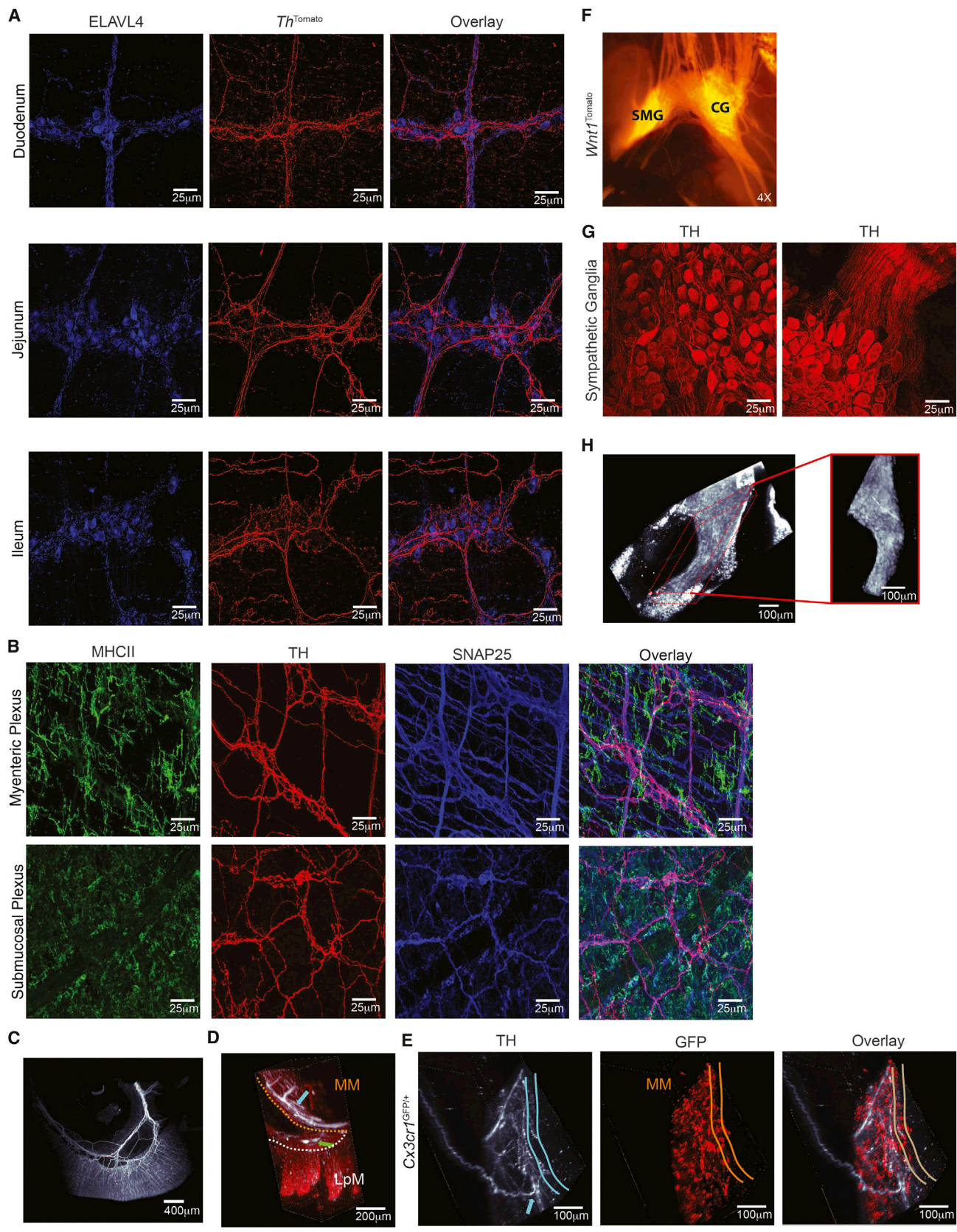
To investigate whether interaction with neurons is sufficient to directly modulate gene expression in macrophages, we first developed an in vitro co-culture system using neurosphere-derived primary enteric-associated neurons and either peritoneal macrophages or a macrophage cell line (RAW 264). Co-culture of RAW 264 macrophages or peritoneal macrophages with primary EANs resulted in increased levels of *Arg1* and *Chi3l3* expression with no change in *Nos2* or *Tnf* expression (Figures 7A–7C). The supernatant of macrophage-EAN co-cultures (conditioned media), but not EAN or macrophage media alone, was also able to induce *Arg1* in macrophages, indicating that, at least under these conditions, EANs may require cell-extrinsic signals in order to release soluble factors responsible for macrophage polarization (Figure 7D). Aply, both NE and Salbutamol, a specific  $\beta_2$ AR agonist, directly induced *Arg1* upregulation but did not change *Tnf* expression in peritoneal macrophages (Figure 7E). Furthermore, addition of butaxamine, a selective  $\beta_2$ AR blocker, prevented *Arg1* upregulation in macrophages co-cultured with EANs (Figure 7F). In these settings, however, we were unable to detect gene changes in additional M2-genes associated with the MM profile (data not shown). These findings reveal that enteric neurons and  $\beta_2$ AR ligands can induce macrophage polarization in vitro resembling MMs.

We next asked whether  $\beta_2$ AR-mediated signaling contributes to in vivo MM polarization after intestinal infection. Previous studies have reported anti-inflammatory effects of  $\beta_2$ AR signaling on macrophages, possibly mediated by upregulation of M2-related genes upon exposure to  $\beta_2$ AR agonists (Spengler et al., 1994). In vivo administration of butaxamine significantly impaired upregulation of *Arg1* and *Chi3l3* (Figure 7G). To further address the role of  $\beta_2$ ARs in this pathway, we also analyzed beta-adrenergic receptor null mice. MMs isolated from *Adrb1<sup>+/-</sup> Adrb2<sup>-/-</sup>* exhibited markedly reduced expression of *Arg1* and *Chi3l3* relative to MMs isolated from *Adrb1/2<sup>+/-</sup>* littermate controls upon *Spib* infection (Figure 7H). The above data provide evidence that enteric infection triggers changes in MM gene expression via neuron-derived adrenergic signaling. Altogether, our results reveal communication between enteric-associated neurons and macrophages in the muscularis microenvironment that serves to induce a tissue-protective gene-expression program in resident macrophages.

## DISCUSSION

### Dynamics of Enteric Neuron-Macrophage Interaction

Tissue-resident macrophages adapt to distinct niches to perform protective, reparative, or pro-inflammatory functions



(legend on next page)

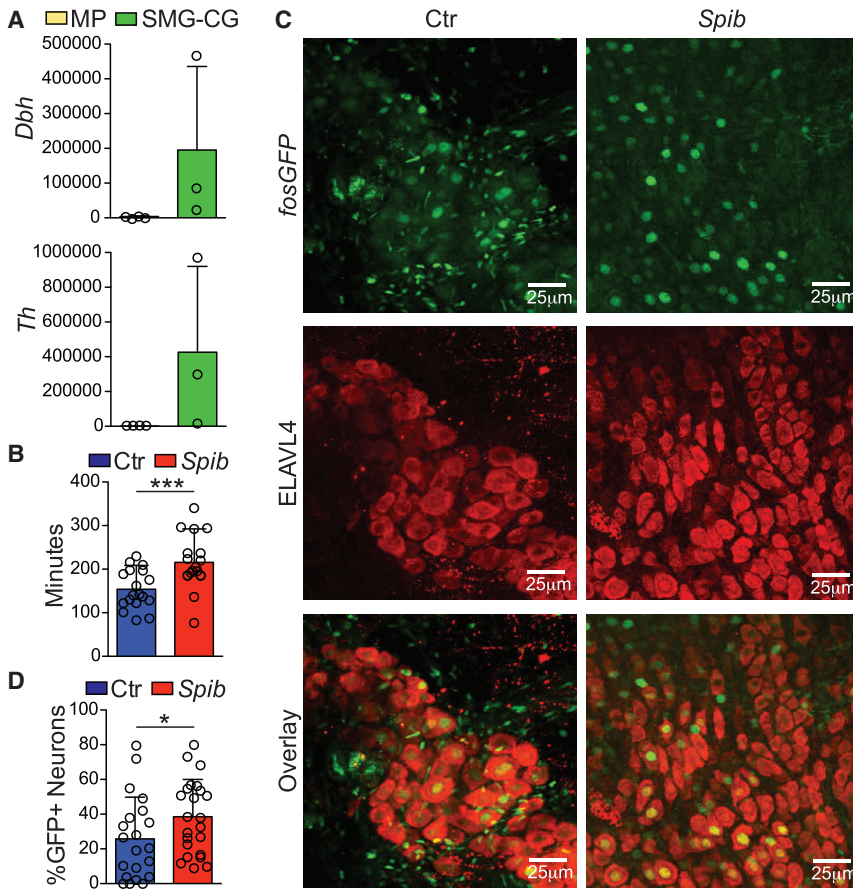


**Figure 6. Extrinsic Sympathetic Innervation Is Activated during Enteric Infection**

(A) Expression of polysome-associated mRNA from small intestine muscularis and SMG-CG of naive *Snap25<sup>RiboTag</sup>* mice determined by qPCR, presented relative to *Hprt*. Pooled data shown are from three independent experiments, n = 3. (B) Total GI transit time (time required to expel feces containing carmine red dye) in mice 30 min post-intragastric exposure to *Spib* or PBS (control). Pooled data shown are from four independent experiments, n = 18. (C) Confocal images from the SMG-CG isolated from *Fos<sup>GFP</sup>* mice 2 hr post-*Spib* intragastric exposure and stained using anti-GFP (upper panels) and anti-ELAVL4 (middle panels) antibodies. Images are representative of two independent experiments, n = 6. (D) Quantification of the number of GFP<sup>+</sup> nuclei among ELAVL4<sup>+</sup>-TH<sup>+</sup> neurons within SMG-CG. Pooled data shown are from two independent experiments, n = 6 (each dot represents one image of sympathetic ganglion neurons). Data were analyzed by unpaired t test and are shown as average ± SD; \*p < 0.05, \*\*\*p < 0.001. See also Figure S4.

depending on their environmental cues and epigenetic state (Lavin et al., 2014; Okabe and Medzhitov, 2014). In the intestinal tissue, tissue macrophages are constantly exposed to both exogenous stimuli, such as bacteria and viruses and endogenous stimuli, which can be membrane-bound or secreted stress molecules from diverse neighboring hematopoietic and stromal cells (Diehl et al., 2013; Farache et al., 2013). Several lines of ev-

idence suggest that the enteric nervous system can directly communicate with MMs. Electron microscopy and immune staining-based studies have suggested that MMs form synapses with enteric neurons (Kinoshita et al., 2007; Phillips and Powley, 2012). Recent work by Muller et al. (2014) has indicated that MMs directly regulate the activity of enteric neurons and peristalsis via secretion of BMP-2 in a microbiota-dependent manner. We provide evidence for reciprocal neuron-dependent macrophage adaptation to environmental perturbations in the intestinal muscularis, where macrophages represent the main hematopoietic lineage (Bogunovic et al., 2009) and share a niche

**Figure 5. Catecholaminergic Innervation of the Intestinal Muscularis**

(A) Confocal images from the duodenum (upper panels), jejunum (middle panels) and ileum (lower panels) isolated from naive *Th<sup>Cre</sup>Rosa26<sup>Isl1-tdTomato</sup>* (*Th<sup>Tomato</sup>*) mice and stained using anti-ELAVL4 (HuC/D) antibodies. Images are representative of at least two independent experiments with sections obtained from duodenum, jejunum, and ileum. (B) Confocal images from the myenteric (upper panels) and submucosal plexuses (lower panels) isolated from naive WT mice and stained using anti-MHCII, anti-SNAP25 and anti-TH antibodies. Images are representative of at least two independent experiments with sections obtained from duodenum, jejunum, and ileum. (C) Whole-mount imaging (iDISCO) from the ileum isolated from naive WT mouse stained using anti-TH (white) antibodies (see also Movie S3A). Images are representative of at least two independent experiments with sections obtained from duodenum, jejunum, and ileum. (D and E) iDISCO from the ileum isolated from *Cx3cr1<sup>GFP/+</sup>* reporter mouse stained using anti-GFP (red) and anti-TH (white) antibodies. (D) Arrows indicate TH<sup>+</sup> processes in the myenteric (light blue) and submucosal (green) plexuses (see also Movie S3B). (E) Light blue arrow indicates TH<sup>+</sup> processes innervating the myenteric plexus (see also Movie S3C). Images are representative of at least two independent experiments with sections obtained from duodenum, jejunum, and ileum. (F) Epifluorescent imaging from the celiac (CG) and superior mesenteric ganglia (SMG) of *Wnt1<sup>Cre</sup>Rosa26<sup>Isl1-tdTomato</sup>* (*Wnt1<sup>Tomato</sup>*) mice. Images are representative of at least two independent experiments with sections obtained from duodenum, jejunum, and ileum. (G) Confocal images from the CG isolated from naive WT mice and stained using anti-TH antibodies. Left: TH<sup>+</sup> cell bodies. Right: TH<sup>+</sup> cell bodies and processes. Images are representative of at least two independent experiments. (H) iDISCO from the CG isolated from WT mouse stained using anti-ELAVL4 antibody, showing the ganglion and the surrounding fat tissue (see also Movie S3D). Image is representative of at least 14 independent experiments. See also Figure S3 and Movie S3.

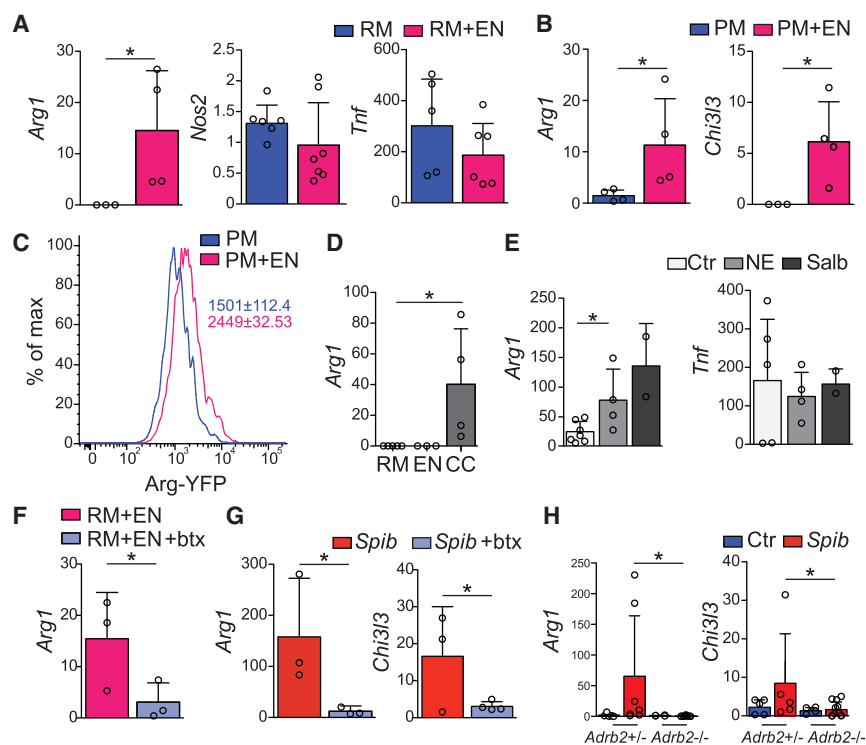


**Figure 7.  $\beta$ 2ARs Mediate Polarization of Macrophages**

(A–F) WT mice neuro-sphere-derived primary enteric-associated neurons (EANS) were co-cultured with RAW (RM) or peritoneal macrophages (PM). (A and B) Expression of mRNA for *Arg1*, *Nos2*, *Tnf*, and *Chi3i3* by sorted (A) RM or (B) PM 24 hr post-co-culture with EANS. (C) Representative flow cytometry histogram for YFP expression by sorted PM isolated from *Arg1*<sup>YFP</sup> mice cultured with EANS as in (A). (D) Expression of mRNA for *Arg1* by sorted RM 24 hr post-exposure to conditioned media from RM, EANS, or RM-EANS co-cultures (CC). (E) Expression of mRNA for *Arg1* and *Tnf* by sorted PM 1 hr post-exposure to NE or Salbutamol ( $\beta$ 2AR agonists). (F) Expression of mRNA for *Arg1* by sorted RM 24 hr post-co-culture with EANS with or without butaxamine ( $\beta$ 2AR-selective blocker). Pooled data of at least two independent experiments. (A)  $n = 3-7$ ; (B–D)  $n = 3-4$ ; (E)  $n = 2-4$ ; (F)  $n = 3-4$ ). Data were analyzed by unpaired t test and are shown as average  $\pm$  SD; \* $p \leq 0.05$ .

(G) Expression of mRNA for *Arg1* and *Chi3i3* by sorted small intestine MMs isolated 2 hr post-intragastric exposure to *Spib* in mice treated with vehicle or butaxamine.

(H) Expression of mRNA for *Arg1* and *Chi3i3* by sorted small intestine MMs isolated from *Adrb1*<sup>+/-</sup>*Adrb2*<sup>-/-</sup> and *Adrb1*<sup>+/-</sup>*Adrb2*<sup>+/-</sup> littermate

control mice 2 hr post-intragastric exposure to *Spib*. qPCR results are presented relative to *Rpl32* expression. Pooled data of at least two independent experiments ( $n = 4-11$ ). Data were analyzed by unpaired t test and are shown as average  $\pm$  SD; \* $p \leq 0.05$ .

See also Figure S2.

with a dense network of neurons. Our analyses of the in vivo dynamics of neuron-macrophage “structural coupling” under inflammatory conditions provides insights into this complex interaction, with possible implications for disease tolerance (Medzhitov et al., 2012).

While lamina propria macrophages are motile and can directly sense signals derived from invading bacteria or epithelial cell stress responses (Diehl et al., 2013; Farache et al., 2013; Mazzini et al., 2014), macrophages residing in the submucosal layer, and in particular the intestinal muscularis, are less likely to directly sense perturbations from the lumen. At the same time, gastrointestinal infections may lead to long-lasting tissue damage induced by inflammatory cells (Rakoff-Nahoum et al., 2004). Hence, mechanisms that induce tissue-protective functions in resident macrophages are an essential component of responses to pathogens (Medzhitov et al., 2012). This might be of particular importance to tissues that include cells with reduced proliferative or regenerative capacity, such as neurons. The static position of MMs, primarily alongside neuronal cell bodies and nerve fibers, provides an optimal interface for such interaction. It is curious to note that the cell dynamics of the bipolar and stellate cells appear to match the structure to which they are most closely associated. For instance, bipolar cells, running parallel to nerve fibers, extend in only two directions and have small pseudopodial protrusions. Stellate MMs, which surround ganglia and neuronal cell bodies, can presumably completely embrace their surrounding area. These features

suggest that MMs below the serosa are involved in the monitoring of neuronal status either through detection of electrical activity or secreted factors, such as CSF-1 (Muller et al., 2014). In these ways, the  $\beta$ 2ARs-mediated MM response may represent an analogous activity to that described for microglia in the CNS; protecting closely associated neuronal processes from infection- or inflammation-induced tissue damage (Davalos et al., 2005; El Khoury et al., 2007; Nimmerjahn et al., 2005; Wang et al., 2015). Several of the genes modulated by the  $\beta$ 2AR pathway are known to be involved in tissue-protective functions. For instance, Arginase 1 has been implicated in the development of the nervous system, axogenesis, and neuroregeneration, as well as anti-apoptotic effects on neurons (Cai et al., 2002; Estévez et al., 2006). Thereby, overt inflammation coupled with disruption of this pathway may lead to tissue damage. Indeed, clinical observations indicate that  $\sim 10\%$  of irritable bowel syndrome (IBS) patients developed symptoms after episodes of gastrointestinal infection (GI) (Ohman and Simrén, 2010). It seems plausible that severe or prolonged GI infection could overrun normal safeguards, such as the MM anti-inflammatory program, and damage EAN networks, permanently impacting GI physiology.

### Sensing of Intestinal Insults at Luminal Sites

We observed that bacterial infection leads to activation of extrinsic sympathetic ganglia innervating the intestine. How do intrinsic or extrinsic neuronal pathways sense luminal

bacteria? Attenuated strains (Tsolis et al., 1999), which already exhibit a reduced capacity to invade even with streptomycin pretreatment, are expected to have limited interaction with the epithelium. Many different pathways could operate in an epithelial-neuronal sensing mechanism. For instance, Wilson et al. (2013) have shown that epithelial cell-derived cytokine thymic stromal lymphopoietin (TSLP), upregulated during allergic responses, is sensed by afferent neurons to trigger itch behavior. In the intestine, where epithelial cells are the source of more than 50% of the body's dopamine and 90% of the body's serotonin, it is very likely that enteroendocrine epithelial cells play an important role in communicating luminal perturbations to neuronal processes (Gershon and Tack, 2007). A recent report by Bohórquez et al. (2015) indicated that intestinal enteroendocrine cells directly connect with neurons innervating the small intestine and colon, possibly providing signals received from the lumen. An alternative, albeit non-mutually exclusive, possibility is that neuronal processes reaching the intestinal villi directly sense microbial or stress signals, as recently shown in worms. Meisel et al. (2014) described a chemosensory mechanism used by *Caenorhabditis elegans* to detect bacterial metabolites and induce avoidance behavior. This pathway involves direct neuronal sensing of pathogenic stimuli, which in turn activates adjacent neurons (Meisel et al., 2014). In mammals, Chiu et al. (2013) showed that sensory neurons could directly respond to bacterial-derived N-formylated peptides or toxins, inducing pain. In this study, ablation of nociceptors resulted in increased inflammatory infiltrate, suggesting an anti-inflammatory role for this pathway during bacterial infection (Chiu et al., 2013). An analogous pathway could be operational in the intestine, where potentially similar metabolites from commensal or invading bacteria would directly activate enteric neurons. Indeed, studies have suggested that enteric neurons express PRRs, such as TLR2 or TLR4 (Anitha et al., 2012) that can contribute to activation of nociceptive-associated channels in neurons such as TRPV1. Alternatively, TLR ligands may be able to directly activate these channels independent of TLRs (Meseguier et al., 2014). However, this sensing circuit still requires further studies specifically targeting PRR pathways or other potential direct sensing channels or receptors in EAN.

### Regulation of Inflammatory Responses by the Catecholamine- $\beta_2$ AR Pathway

In addition to the well-described anti-inflammatory reflex, the involvement of catecholaminergic neurons in anti-inflammatory responses has many equivalents in the immune system (Tracey, 2009). However, catecholamines are also linked to enhanced inflammatory responses. It is thought that  $\alpha$ -adrenergic signaling boosts inflammation while  $\beta$ -adrenergic signaling suppresses both innate and adaptive immunity (Guereschi et al., 2013; Nakai et al., 2014). Some of the broad anti-inflammatory effects of this pathway are attributed to widespread sympathetic innervation in peripheral lymph nodes associated with expression of  $\beta_2$ AR in immune cells (del Rey and Besedovsky, 2008). The high expression of these receptors by MMs might represent a mechanism by which heavy norepinephrine innervation in the muscularis could preferentially target these cells, mitigating the pro-inflammatory state induced in LpMs close to the lumen. Plausibly, deep

muscular and myenteric macrophages are in a privileged position to respond to neuronal signals, including NE, due to their contact with neuronal fibers, as opposed to their serosa-longitudinal muscle counterparts. Alternatively, lack of  $\beta_2$ AR on neurons or another cell population may lead to a decrease in a necessary support factor in these areas. Similarly, subpopulations of B cells, macrophages and neutrophils preferentially express  $\beta_2$ AR when compared to T cells (del Rey and Besedovsky, 2008), which could also explain how NE might regulate inflammatory responses without leading to immune suppression. Additionally, circulating levels of NE, as opposed to much higher concentrations around catecholaminergic nerve terminals comprise an additional layer of control of this MM-EAN-associated NE- $\beta_2$ AR axis (del Rey and Besedovsky, 2008). Although we found TH<sup>+</sup> immunoreactivity within the intestinal muscularis as well as in the SMG-CG, we only observed activation of extrinsic innervation upon bacterial challenge. This is consistent with previous reports suggesting that the CG and SMG are the main sources of NE in the stomach and intestine (Li et al., 2010). Nevertheless, we cannot rule out the possibility that intrinsic innervation is also involved in this process since extrinsic innervation synapses directly onto EAN, and this could also be involved in sensing mechanisms (McVey Neufeld et al., 2015).

The hardwiring of lymphoid and non-lymphoid tissues with neuronal processes allows for immediate regulation of closely-associated cells, and this could potentially synchronize immune responses in areas not directly in contact with the stimuli. We have uncovered a neuro-immune axis that reinforces a tissue-protective program in macrophages in response to a potentially pathogenic insult. Future studies are needed to dissect the exact (afferent and efferent) roles played by EAN in this process. Additionally, it remains unclear how luminal signals reach intrinsic or extrinsic innervation. Exploring these questions are the next steps to understanding how neuronal hardwiring in the intestine and other immune-rich tissues can modulate immune responses and how immune cells may prevent or cause neuronal damage.

### EXPERIMENTAL PROCEDURES

#### Animals

*Arg*<sup>YFP</sup>(*Arg1*<sup>tm1Lky/J</sup>), *Adrb1*<sup>tm1Bkk</sup>*Adrb2*<sup>tm1Bkk</sup>, C57BL/6J, *Cx3cr1*<sup>GFP</sup>(*Cx3cr1*<sup>tm1Litt/Litt</sup>), *Rosa26*<sup>Isl-GCaMP3</sup>(Gt(ROSA)26Sortm38(CAG-GCaMP3)Hze), *Rosa26*<sup>Isl-tomato</sup>(Gt(ROSA)26Sortm9(CAG-tdTomato)Hze), *Itgax*(CD11c)<sup>eYFP</sup>, *Lyz2*<sup>Cre/Cre</sup>(*Lyz2*<sup>tm1(cre)lfo/J</sup>), *Fos*<sup>GFP</sup>(B6.Cg-Tg(Fos/EGFP)1-3Brth/J), *Snap25*<sup>Cre</sup>(*Snap25*<sup>tm2.1(cre)Hze</sup>), *Rpl22*<sup>tm1.1Psam/J</sup>, *Wnt1*<sup>Cre</sup>(Tg(Wnt1-cre)2Sor), and *zDC*<sup>DTR</sup>(*Zbtb46*<sup>DTR</sup>) mice were purchased from the Jackson Laboratories and maintained in our facilities. *Hand2*<sup>Cre</sup>(Tg(Hand2-cre)7-1Clou) and *Th*<sup>Cre</sup>(Tg(Th-cre)1Tmd), mice were generously provided by D. Clouthier (UC Denver) and J. Friedman (RU), respectively. These lines were interbred in our facilities to obtain the final strains described in the text. Genotyping was performed according to the protocols established for the respective strains by Jackson Laboratories. Mice were maintained at the Rockefeller University animal facilities under specific pathogen-free conditions. Mice were used at 7–12 weeks of age for most experiments. Animal care and experimentation were consistent with the NIH guidelines and were approved by the Institutional Animal Care and Use Committee at the Rockefeller University.

#### iDISCO

The iDISCO protocol was followed as detailed on the continuously-updated website: <http://idisco.info>. For more detailed information, please see the Supplemental Experimental Procedures.

### Intravital Two-Photon Imaging

Images were acquired as previously described (Farache et al., 2013). For more detailed information, please see the [Supplemental Experimental Procedures](#).

### RiboTag

Isolation of HA-tagged polysomes was performed as previously described (Sanz et al., 2009). For more detailed information, please see the [Supplemental Experimental Procedures](#).

### Single Cell Suspension of Intestinal Macrophages

After cleaning and washing in HBSS, the small intestine tissue was cut in two and the muscularis region was carefully dissected from the underlying mucosa. For more detailed information, please see the [Supplemental Experimental Procedures](#).

### Salmonella Typhimurium Infections

Mice were intragastrically exposed to  $10^9$  of either mutant strain of *Salmonella* Typhimurium, *Spib*, or *invA*. For more detailed information, please see the [Supplemental Experimental Procedures](#).

### Statistics

Statistical analyses were performed in GraphPad Prism software. Data were analyzed by applying one-way ANOVA or unpaired Student's t test where appropriate. A p value < 0.05 was considered significant.

For additional detailed information, please see the [Supplemental Experimental Procedures](#).

### ACCESSION NUMBERS

The accession number for all RNA-seq data reported in this paper is NCBI Gene Expression Omnibus (GEO): GSE74131.

### SUPPLEMENTAL INFORMATION

Supplemental Information includes Supplemental Experimental Procedures, four figures, one table, and three movies and can be found with this article online at <http://dx.doi.org/10.1016/j.cell.2015.12.023>.

### AUTHOR CONTRIBUTIONS

D.M. conceived and supervised this study. I.G., P.A.M., F.A.C.-P., and D.M. designed experiments. I.G., P.A.M., L.F., and F. A.C.-P. performed experiments. I.G. and P.A.M. prepared figures and helped with manuscript preparation. T.Y.O. analyzed RNA-seq and helped with figure preparation. D.M. wrote the paper.

### ACKNOWLEDGMENTS

We are indebted to K. Velinon and N. Thomas for sorting cells, P. Ariel and the Rockefeller University Bio-Imaging Resource Center (BIRC) for their invaluable help with IVM and light sheet microscopy, N. Renier and R. Azevedo for their help with the iDISCO, D. Esterházy for kindly providing *Ly22<sup>csfr1-DTR</sup>CD11c<sup>eYFP</sup>* mice, M. Bogunovic and M. Merad (Mount Sinai) for their insightful discussions and help with the isolation of MMs and LpMs, J. Farache, G. Shakhar (Weizmann), and G. Victoria (Whitehead, MIT) for their help in establishing live multiphoton microscopy of the gut, members of the Nussenzweig lab and The Rockefeller University employees for continuous assistance. We thank S. Tavazoei, V. Ruta, M. Nussenzweig (RU) and members of our laboratory, particularly V. Pedicord for discussions and critical reading and editing of the manuscript. D.M. is supported by a Kenneth Rainin Foundation Breakthrough Award, a National Institutes of Health NIH 5R21AI105047 grant. D.M. and P.A.M. are supported by the Leona M. and Harry B. Helmsley Charitable Trust. L.F. was supported by Crohn's and Colitis Foundation of America. I.G. and F.A.C.-P. were supported by FAPESP and CNPq (Brazil). The BIRC is supported by the Empire State Stem Cell Fund through NYSDOH C023046.

Received: October 19, 2015

Revised: November 24, 2015

Accepted: December 4, 2015

Published: January 14, 2016

### REFERENCES

- Anitha, M., Vijay-Kumar, M., Sitaraman, S.V., Gewirtz, A.T., and Srinivasan, S. (2012). Gut microbial products regulate murine gastrointestinal motility via Toll-like receptor 4 signaling. *Gastroenterology* *143*, 1006–1016.
- Ayres, J.S., Trinidad, N.J., and Vance, R.E. (2012). Lethal inflammasome activation by a multidrug-resistant pathobiont upon antibiotic disruption of the microbiota. *Nat. Med.* *18*, 799–806.
- Barron, F., Woods, C., Kuhn, K., Bishop, J., Howard, M.J., and Clouthier, D.E. (2011). Downregulation of *Dlx5* and *Dlx6* expression by *Hand2* is essential for initiation of tongue morphogenesis. *Development* *138*, 2249–2259.
- Bogunovic, M., Ginhoux, F., Helft, J., Shang, L., Hashimoto, D., Greter, M., Liu, K., Jakubzick, C., Ingersoll, M.A., Leboeuf, M., et al. (2009). Origin of the lamina propria dendritic cell network. *Immunity* *31*, 513–525.
- Bohórquez, D.V., Shahid, R.A., Erdmann, A., Kreger, A.M., Wang, Y., Calakos, N., Wang, F., and Liddle, R.A. (2015). Neuroepithelial circuit formed by innervation of sensory enteroendocrine cells. *J. Clin. Invest.* *125*, 782–786.
- Cai, D., Deng, K., Mellado, W., Lee, J., Ratan, R.R., and Filbin, M.T. (2002). Arginase I and polyamines act downstream from cyclic AMP in overcoming inhibition of axonal growth MAG and myelin in vitro. *Neuron* *35*, 711–719.
- Chiu, I.M., Heesters, B.A., Ghasemlou, N., Von Hehn, C.A., Zhao, F., Tran, J., Wainger, B., Strominger, A., Muralidharan, S., Horswill, A.R., et al. (2013). Bacteria activate sensory neurons that modulate pain and inflammation. *Nature* *501*, 52–57.
- Danielian, P.S., Muccino, D., Rowitch, D.H., Michael, S.K., and McMahon, A.P. (1998). Modification of gene activity in mouse embryos in utero by a tamoxifen-inducible form of Cre recombinase. *Curr. Biol.* *8*, 1323–1326.
- Davalos, D., Grutzendler, J., Yang, G., Kim, J.V., Zuo, Y., Jung, S., Littman, D.R., Dustin, M.L., and Gan, W.B. (2005). ATP mediates rapid microglial response to local brain injury in vivo. *Nat. Neurosci.* *8*, 752–758.
- del Rey, A., and Besedovsky, H.O. (2008). Sympathetic nervous system-immune interactions in autoimmune lymphoproliferative diseases. *Neuroimmunomodulation* *15*, 29–36.
- Denning, T.L., Wang, Y.C., Patel, S.R., Williams, I.R., and Pulendran, B. (2007). Lamina propria macrophages and dendritic cells differentially induce regulatory and interleukin 17-producing T cell responses. *Nat. Immunol.* *8*, 1086–1094.
- Diehl, G.E., Longman, R.S., Zhang, J.X., Breart, B., Galan, C., Cuesta, A., Schwab, S.R., and Littman, D.R. (2013). Microbiota restricts trafficking of bacteria to mesenteric lymph nodes by CX(3)CR1(hi) cells. *Nature* *494*, 116–120.
- El Khoury, J., Toft, M., Hickman, S.E., Means, T.K., Terada, K., Geula, C., and Luster, A.D. (2007). *Ccr2* deficiency impairs microglial accumulation and accelerates progression of Alzheimer-like disease. *Nat. Med.* *13*, 432–438.
- Estévez, A.G., Sahawneh, M.A., Lange, P.S., Bae, N., Egea, M., and Ratan, R.R. (2006). Arginase 1 regulation of nitric oxide production is key to survival of trophic factor-deprived motor neurons. *J. Neurosci.* *26*, 8512–8516.
- Farache, J., Koren, I., Milo, I., Gurevich, I., Kim, K.W., Zsigmond, E., Furtado, G.C., Lira, S.A., and Shakhar, G. (2013). Luminal bacteria recruit CD103+ dendritic cells into the intestinal epithelium to sample bacterial antigens for presentation. *Immunity* *38*, 581–595.
- Furness, J.B., Kunze, W.A., and Clerc, N. (1999). Nutrient tasting and signaling mechanisms in the gut. II. The intestine as a sensory organ: neural, endocrine, and immune responses. *Am. J. Physiol.* *277*, G922–G928.
- Gautier, E.L., Shay, T., Miller, J., Greter, M., Jakubzick, C., Ivanov, S., Helft, J., Chow, A., Elpek, K.G., Gordonov, S., et al.; Immunological Genome Consortium (2012). Gene-expression profiles and transcriptional regulatory pathways that underlie the identity and diversity of mouse tissue macrophages. *Nat. Immunol.* *13*, 1118–1128.

- Gershon, M.D., and Tack, J. (2007). The serotonin signaling system: from basic understanding to drug development for functional GI disorders. *Gastroenterology* *132*, 397–414.
- Ghisletti, S., Barozzi, I., Mietton, F., Polletti, S., De Santa, F., Venturini, E., Gregory, L., Lonie, L., Chew, A., Wei, C.L., et al. (2010). Identification and characterization of enhancers controlling the inflammatory gene expression program in macrophages. *Immunity* *32*, 317–328.
- Guereschi, M.G., Araujo, L.P., Maricato, J.T., Takenaka, M.C., Nascimento, V.M., Vivanco, B.C., Reis, V.O., Keller, A.C., Brum, P.C., and Basso, A.S. (2013). Beta2-adrenergic receptor signaling in CD4<sup>+</sup> Foxp3<sup>+</sup> regulatory T cells enhances their suppressive function in a PKA-dependent manner. *Eur. J. Immunol.* *43*, 1001–1012.
- Hadis, U., Wahl, B., Schulz, O., Hardtke-Wolenski, M., Schippers, A., Wagner, N., Müller, W., Sparwasser, T., Förster, R., and Pabst, O. (2011). Intestinal tolerance requires gut homing and expansion of FoxP3<sup>+</sup> regulatory T cells in the lamina propria. *Immunity* *34*, 237–246.
- Harris, J.A., Hirokawa, K.E., Sorensen, S.A., Gu, H., Mills, M., Ng, L.L., Bohn, P., Mortrud, M., Ouellette, B., Kidney, J., et al. (2014). Anatomical characterization of Cre driver mice for neural circuit mapping and manipulation. *Front. Neural Circuits* *8*, 76.
- Hashimoto, D., Chow, A., Noizat, C., Teo, P., Beasley, M.B., Leboeuf, M., Becker, C.D., See, P., Price, J., Lucas, D., et al. (2013). Tissue-resident macrophages self-maintain locally throughout adult life with minimal contribution from circulating monocytes. *Immunity* *38*, 792–804.
- Hendershot, T.J., Liu, H., Sarkar, A.A., Giovannucci, D.R., Clouthier, D.E., Abe, M., and Howard, M.J. (2007). Expression of Hand2 is sufficient for neurogenesis and cell type-specific gene expression in the enteric nervous system. *Dev. Dyn.* *236*, 93–105.
- Kinoshita, K., Horiguchi, K., Fujisawa, M., Kobirumaki, F., Yamato, S., Hori, M., and Ozaki, H. (2007). Possible involvement of muscularis resident macrophages in impairment of interstitial cells of Cajal and myenteric nerve systems in rat models of TNBS-induced colitis. *Histochem. Cell Biol.* *127*, 41–53.
- Lavin, Y., Winter, D., Blecher-Gonen, R., David, E., Keren-Shaul, H., Merad, M., Jung, S., and Amit, I. (2014). Tissue-resident macrophage enhancer landscapes are shaped by the local microenvironment. *Cell* *159*, 1312–1326.
- Li, Z., Caron, M.G., Blakely, R.D., Margolis, K.G., and Gershon, M.D. (2010). Dependence of serotonergic and other nonadrenergic enteric neurons on norepinephrine transporter expression. *J. Neurosci.* *30*, 16730–16740.
- Mazzini, E., Massimiliano, L., Penna, G., and Rescigno, M. (2014). Oral tolerance can be established via gap junction transfer of fed antigens from CX3CR1<sup>+</sup> macrophages to CD103<sup>+</sup> dendritic cells. *Immunity* *40*, 248–261.
- McVey Neufeld, K.A., Perez-Burgos, A., Mao, Y.K., Bienenstock, J., and Kunze, W.A. (2015). The gut microbiome restores intrinsic and extrinsic nerve function in germ-free mice accompanied by changes in calbindin. *Neurogastroenterol. Motil.* *27*, 627–636.
- Medzhitov, R., Schneider, D.S., and Soares, M.P. (2012). Disease tolerance as a defense strategy. *Science* *335*, 936–941.
- Meisel, J.D., Panda, O., Mahanti, P., Schroeder, F.C., and Kim, D.H. (2014). Chemosensation of bacterial secondary metabolites modulates neuroendocrine signaling and behavior of *C. elegans*. *Cell* *159*, 267–280.
- Meseguer, V., Alpizar, Y.A., Luis, E., Tajada, S., Denlinger, B., Fajardo, O., Manenschijn, J.A., Fernández-Peña, C., Talavera, A., Kichko, T., et al. (2014). TRPA1 channels mediate acute neurogenic inflammation and pain produced by bacterial endotoxins. *Nat. Commun.* *5*, 3125.
- Muller, P.A., Koscsó, B., Rajani, G.M., Stevanovic, K., Berres, M.L., Hashimoto, D., Mortha, A., Leboeuf, M., Li, X.M., Mucida, D., et al. (2014). Crosstalk between muscularis macrophages and enteric neurons regulates gastrointestinal motility. *Cell* *158*, 300–313.
- Nakai, A., Hayano, Y., Furuta, F., Noda, M., and Suzuki, K. (2014). Control of lymphocyte egress from lymph nodes through  $\beta$ 2-adrenergic receptors. *J. Exp. Med.* *211*, 2583–2598.
- Nguyen, K.D., Qiu, Y., Cui, X., Goh, Y.P., Mwangi, J., David, T., Mukundan, L., Brombacher, F., Locksley, R.M., and Chawla, A. (2011). Alternatively activated macrophages produce catecholamines to sustain adaptive thermogenesis. *Nature* *480*, 104–108.
- Niess, J.H., Brand, S., Gu, X., Landsman, L., Jung, S., McCormick, B.A., Vyas, J.M., Boes, M., Ploegh, H.L., Fox, J.G., et al. (2005). CX3CR1-mediated dendritic cell access to the intestinal lumen and bacterial clearance. *Science* *307*, 254–258.
- Nimmerjahn, A., Kirchhoff, F., and Helmchen, F. (2005). Resting microglial cells are highly dynamic surveillants of brain parenchyma in vivo. *Science* *308*, 1314–1318.
- Ohman, L., and Simrén, M. (2010). Pathogenesis of IBS: role of inflammation, immunity and neuroimmune interactions. *Nat. Rev. Gastroenterol. Hepatol.* *7*, 163–173.
- Okabe, Y., and Medzhitov, R. (2014). Tissue-specific signals control reversible program of localization and functional polarization of macrophages. *Cell* *157*, 832–844.
- Parkhurst, C.N., Yang, G., Ninan, I., Savas, J.N., Yates, J.R., 3rd, Lafaille, J.J., Hempstead, B.L., Littman, D.R., and Gan, W.B. (2013). Microglia promote learning-dependent synapse formation through brain-derived neurotrophic factor. *Cell* *155*, 1596–1609.
- Phillips, R.J., and Powley, T.L. (2012). Macrophages associated with the intrinsic and extrinsic autonomic innervation of the rat gastrointestinal tract. *Auton. Neurosci.* *169*, 12–27.
- Pullinger, G.D., van Diemen, P.M., Carnell, S.C., Davies, H., Lyte, M., and Stevens, M.P. (2010). 6-hydroxydopamine-mediated release of norepinephrine increases faecal excretion of *Salmonella enterica* serovar Typhimurium in pigs. *Vet. Res.* *41*, 68.
- Råberg, L., Sim, D., and Read, A.F. (2007). Disentangling genetic variation for resistance and tolerance to infectious diseases in animals. *Science* *318*, 812–814.
- Rakoff-Nahoum, S., Paglino, J., Eslami-Varzaneh, F., Edberg, S., and Medzhitov, R. (2004). Recognition of commensal microflora by toll-like receptors is required for intestinal homeostasis. *Cell* *118*, 229–241.
- Renier, N., Wu, Z., Simon, D.J., Yang, J., Ariel, P., and Tessier-Lavigne, M. (2014). iDISCO: a simple, rapid method to immunolabel large tissue samples for volume imaging. *Cell* *159*, 896–910.
- Sanz, E., Yang, L., Su, T., Morris, D.R., McKnight, G.S., and Amieux, P.S. (2009). Cell-type-specific isolation of ribosome-associated mRNA from complex tissues. *Proc. Natl. Acad. Sci. USA* *106*, 13939–13944.
- Schreiber, H.A., Loschko, J., Karssemeijer, R.A., Escolano, A., Meredith, M.M., Mucida, D., Guermonez, P., and Nussenzweig, M.C. (2013). Intestinal monocytes and macrophages are required for T cell polarization in response to *Citrobacter rodentium*. *J. Exp. Med.* *210*, 2025–2039.
- Soares, M.P., Gozzelino, R., and Weis, S. (2014). Tissue damage control in disease tolerance. *Trends Immunol.* *35*, 483–494.
- Spengler, R.N., Chensue, S.W., Giacherio, D.A., Blenk, N., and Kunkel, S.L. (1994). Endogenous norepinephrine regulates tumor necrosis factor- $\alpha$  production from macrophages in vitro. *J. Immunol.* *152*, 3024–3031.
- Tracey, K.J. (2009). Reflex control of immunity. *Nat. Rev. Immunol.* *9*, 418–428.
- Tsolis, R.M., Townsend, S.M., Miao, E.A., Miller, S.I., Ficht, T.A., Adams, L.G., and Bäumler, A.J. (1999). Identification of a putative *Salmonella enterica* serotype typhimurium host range factor with homology to IpaH and YopM by signature-tagged mutagenesis. *Infect. Immun.* *67*, 6385–6393.
- Van Dyken, S.J., and Locksley, R.M. (2013). Interleukin-4- and interleukin-13-mediated alternatively activated macrophages: roles in homeostasis and disease. *Annu. Rev. Immunol.* *31*, 317–343.
- Wang, Y., Szretter, K.J., Vermi, W., Gilfillan, S., Rossini, C., Cella, M., Barrow, A.D., Diamond, M.S., and Colonna, M. (2012). IL-34 is a tissue-restricted ligand of CSF1R required for the development of Langerhans cells and microglia. *Nat. Immunol.* *13*, 753–760.
- Wang, Y., Cella, M., Mallinson, K., Ulrich, J.D., Young, K.L., Robinette, M.L., Gilfillan, S., Krishnan, G.M., Sudhakar, S., Zinselmeyer, B.H., et al. (2015). TREM2 lipid sensing sustains the microglial response in an Alzheimer's disease model. *Cell* *160*, 1061–1071.

Wilson, S.R., Thé, L., Batia, L.M., Beattie, K., Katibah, G.E., McClain, S.P., Pellegrino, M., Estandian, D.M., and Bautista, D.M. (2013). The epithelial cell-derived atopic dermatitis cytokine TSLP activates neurons to induce itch. *Cell* 155, 285–295.

Zariwala, H.A., Borghuis, B.G., Hoogland, T.M., Madisen, L., Tian, L., De Zeeuw, C.I., Zeng, H., Looger, L.L., Svoboda, K., and Chen, T.W. (2012). A

Cre-dependent GCaMP3 reporter mouse for neuronal imaging in vivo. *J. Neurosci.* 32, 3131–3141.

Zigmond, E., Bernshtein, B., Friedlander, G., Walker, C.R., Yona, S., Kim, K.W., Brenner, O., Krauthgamer, R., Varol, C., Müller, W., and Jung, S. (2014). Macrophage-restricted interleukin-10 receptor deficiency, but not IL-10 deficiency, causes severe spontaneous colitis. *Immunity* 40, 720–733.